



## Late Quaternary glacial–interglacial variations in sediment supply in the southern Drake Passage

Jae Il Lee <sup>a,\*</sup>, Ho Il Yoon <sup>a</sup>, Kyu-Cheul Yoo <sup>a</sup>, Hyoun Soo Lim <sup>a</sup>, Yong Il Lee <sup>b</sup>, Donghyun Kim <sup>b</sup>, Young-Suk Bak <sup>c</sup>, Takuya Itaki <sup>d</sup>

<sup>a</sup> Korea Polar Research Institute, Songdo Technopark, 12 Gaetbeol-ro, Songdo-dong, Yeonsu-gu, Incheon 406–840, Republic of Korea

<sup>b</sup> School of Earth and Environmental Sciences, Seoul National University, Seoul 151–742, Republic of Korea

<sup>c</sup> Department of Geology, Kyungpook National University, Daegu 702–701, Republic of Korea

<sup>d</sup> Geological Survey of Japan, National Institute of Advanced Industrial Science and Technology, Higashi 1-1-1, Tsukuba, Ibaraki 305–8567, Japan

### ARTICLE INFO

#### Article history:

Received 29 March 2011

Available online 28 April 2012

#### Keywords:

Quaternary  
Antarctica  
Drake Passage  
Sediment  
Provenance  
Paleoclimate  
Geochemistry

### ABSTRACT

Geochemical characteristics of marine sediment from the southern Drake Passage were analyzed to reconstruct variations in sediment provenance and transport paths during the late Quaternary. The 5.95 m gravity core used in this study records paleoenvironmental changes during the last approximately 600 ka. Down-core variations in trace element, rare earth element, and Nd and Sr isotopic compositions reveal that sediment provenance varied according to glacial cycles. During glacial periods, detrital sediments in the southern Drake Passage were mostly derived from the nearby South Shetland Islands and shelf sediments. In contrast, interglacial sediments are composed of mixed sediments, derived from both West Antarctica and East Antarctica. The East Antarctic provenance of the interglacial sediments was inferred to be the Weddell Sea region. Sediment input from the Weddell Sea was reduced during glacial periods by extensive ice sheets and weakened current from the Weddell Sea. Sediment supply from the Weddell Sea increased during interglacial periods, especially those with higher warmth such as MIS 5, 9, and 11. This suggests that the influence of deep water from the Weddell Sea increases during interglacial periods and decreases during glacial periods, with the degree of influence increasing as interglacial intensity increases.

© 2012 University of Washington. Published by Elsevier Inc. All rights reserved.

### Introduction

The composition of detrital sediments is mainly controlled by source-rock composition, chemical weathering, and transportation (Johnsson, 1993). In polar environments where chemical weathering is weaker, source-rock control on sediment composition is far more important than in other environments and sediment composition is therefore very useful for tracing the source area. Provenance and dispersal of sediments in glacio-marine environments vary according to environmental factors, such as the extent of ice sheets, the strength and direction of ocean circulation, and the dominant depositional processes (e.g., ice rafting, bottom-current deposits). Detrital geochemistry of sediments is not affected by factors controlling the biological proxies, and thus sediment provenance data and biological proxy-based paleoceanographic data can complement each other (Hemming et al., 2007). Glacial–interglacial cycles can be a major control on sediment composition in polar environments on the scale of several hundred thousand to several million years by regulating

ocean circulation and ice-sheet extent, leading to changes in sedimentary provenance.

In the Southern Ocean, only a few studies have dealt with the impact of glacial cycles on the geochemistry of sediments despite the importance of the Southern Ocean in the global climate system (e.g., Bareille et al., 1994; Diekmann et al., 2000; Walter et al., 2000; Hemming et al., 2007). Among these studies, noticeable differences in the geochemistry of sediments between glacial and interglacial periods were reported only in sediments from the Scotia Sea (Diekmann et al., 2000; Walter et al., 2000). Quaternary sediments in the Drake Passage have rarely been studied due to thin sediment cover, with the exception of research by Bae et al. (2003) and Yoon et al. (2009). They reconstructed paleoceanographic changes in the Drake Passage during the last 150 ka using biological proxies, but the provenance of the late Quaternary sediments in the Drake Passage is still largely unknown. The southern Drake Passage is close to the South Shetland Islands (SSI) and the northern Antarctic Peninsula (AP), which are mainly composed of Mesozoic and Cenozoic subduction-related volcanic and plutonic rocks (Saunders et al., 1980; Tarney et al., 1982; Thomson and Pankhurst, 1983; Machado et al., 2005a, 2005b). The relatively simple geology of the nearby source region of the southern Drake Passage allows for the detection of detritus derived from the other regions. In this study we analyzed the geochemical characteristics of the late Quaternary

\* Corresponding author. Fax: +82 32 260 6109.

E-mail address: [leeji@kopri.re.kr](mailto:leeji@kopri.re.kr) (J.I. Lee).

sediments from the southern Drake Passage to detect changes in sediment provenance and sediment dispersal. The variation in detrital geochemistry was compared with glacial-interglacial cycles to understand the effect of glacial cycles on sediment dispersal and paleoceanographic setting in the southern Drake Passage. The studied core also allowed us to compare the geochemistry of interglacial sediments from different stages because it contains a much longer sedimentary record than other Drake Passage cores studied in previous work (Bae et al., 2003; Yoon et al., 2009).

### Oceanographic setting

Since its formation, the Drake Passage has been under the influence of the Antarctic Circumpolar Current (ACC), the largest ocean current in the world, flowing clockwise around Antarctica. Orsi et al. (1995) identified three deep-reaching circumpolar fronts within the ACC: the Subantarctic Front (SAF in Fig. 1), the Polar Front (PF), and the Southern ACC Front (SACCF). The three fronts dominate the total ACC volume transport in the Drake Passage, and the largest transport is observed across the PF (Whitworth et al., 1982; Orsi et al., 1995). The SACCF is not a water mass boundary, but rather the southernmost current core and a part of the ACC (Orsi et al., 1995). The deep-water mass in the Southern Ocean is composed of the clockwise-flowing Circumpolar Deep Water (CDW) and Antarctic Bottom Water. CDW is divided into the Upper

Circumpolar Deep Water (UCDW) and Lower Circumpolar Deep Water (LCDW). The southern boundary of the ACC (SBACC) can be identified using the southern terminus of the UCDW, because the UCDW is found exclusively in the ACC and farther south the observed geostrophic shear is much weaker than within the ACC (Orsi et al., 1995). The SBACC coincides with the northern limits of the Weddell Gyre (Orsi et al., 1995).

In contrast to the generally eastward flowing ACC in the Drake Passage, southwestward flow is observed along the AP continental margin south of the SBACC (Tucholke, 1977; Whitworth et al., 1982; Nowlin and Zenk, 1988; Hillenbrand et al., 2008). Current measurements in the southern Drake Passage confirmed the presence of a persistent westward flow of near-bottom water along the shelf edge and continental slope west of Livingston Island (Whitworth et al., 1982; Nowlin and Zenk, 1988). A relatively cold and fresh branch of Weddell Sea Deep Water (WSDW) and overlying modified LCDW derived from the Warm Deep Water in the Weddell Gyre flow southwestward along the Pacific margin of the AP (Fig. 1; Hernández-Molina et al., 2006). This southwestward bottom current has affected the deposition of the sediment drifts found southwest of the South Shetland Trench on the continental rise west of the AP during at least the last 9.4 Ma (Hillenbrand et al., 2008). Shallow circulation, however, indicates a dominance of northeastward flow on the shelf edge west of the AP, in parallel with the ACC (Fig. 1; Hofmann et al.,

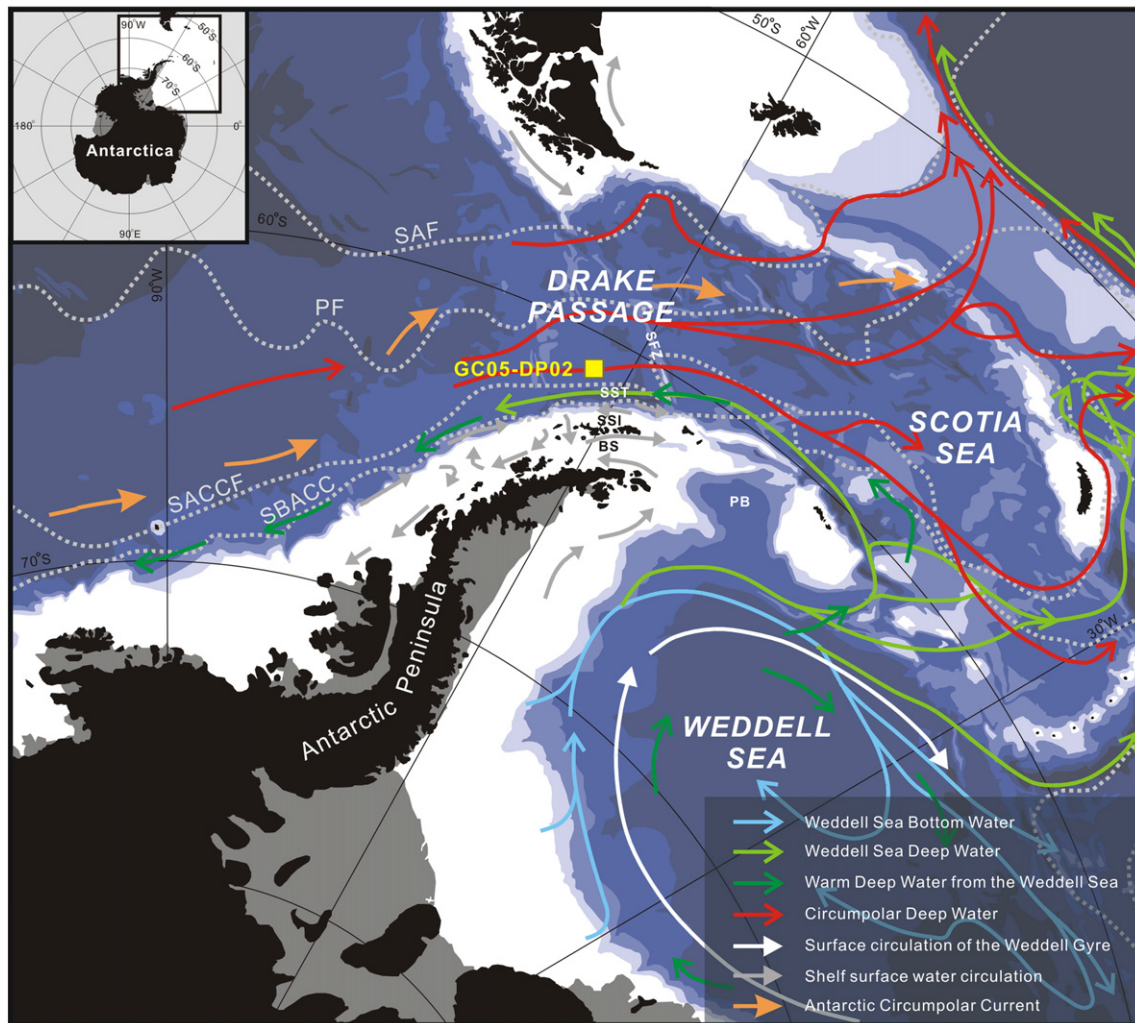


**Figure 1.** Sample location and the oceanographic setting of the study area. Water depths are shown in 1000 m contours. Ice shelves are shown in gray shade. Location of the southern boundary of the Antarctic Circumpolar Current (SBACC), Southern Antarctic Circumpolar Current Front (SACCF), Polar Front (PF), and Subantarctic Front (SAF) is from Orsi et al. (1995). Deep and shallow water circulation paths are from the compilation of Hernández-Molina et al. (2006). Shelf-water circulation on the west of the northern Antarctic Peninsula is from Hofmann et al. (1996). SSI = South Shetland Islands, SST = South Shetland Trench, BS = Bransfield Strait, SFZ = Shackleton Fracture Zone, PB = Powell Basin.

1996; Savidge and Amft, 2009). A southwestward flow, which is probably the shallow component of the southwestward along-slope water from the Weddell Sea, exists on the northern shelf of the SSI, but it does not appear to extend farther south (Hofmann et al., 1996; Savidge and Amft, 2009).

The studied core site is located just north of the SACCF and is under the influence of the eastward flowing ACC (Fig. 1). Nowlin and Zenk (1988) reported a northward flow at 2640 m (water depth) near the core site (their mooring site ML-11). This indicates the influence of the ACC at that depth because the ACC is deflected northward at that location by the Shackleton Fracture Zone. However, it is not certain whether the study area is affected by the southwestward flowing near-bottom current along the slope of the SSI because the flow direction was measured 1114 m above the bottom (Nowlin and Zenk, 1988).

## Materials and methods

Gravity core GC05-DP02 was obtained from the southern Drake Passage (61° 02.7096'S, 62° 38.3859' W, water depth 3503 m, core length 595 cm; Fig. 1) by the R/V *Yuzhmorgeologiya* during the 2005/2006 cruise of the Korea Arctic and Antarctic Research Program. The core was measured for magnetic susceptibility (MS) at 1-cm intervals using a Bartington MS2 susceptibility meter. The core was sampled at every 4 cm for grain size analysis. The content of grains larger than 4 $\phi$  (63  $\mu$ m) was determined by wet sieving, and the content of finer fractions was analyzed using a Micrometrics Sedigraph 5100.

Carbonate preservation in the core is poor, and biogenic carbonate occurs only at 19–73 cm and 148–187 cm. Three planktonic foraminifera samples taken from 32-, 48-, and 64-cm core depths were dated using a radiocarbon AMS dating technique at Rafter Radiocarbon Laboratory. Measured radiocarbon ages were corrected using the apparent age  $585 \pm 40$   $^{14}\text{C}$  yr BP of carbonate shells from the South Shetland Islands as the reservoir age (Gordon and Harkness, 1992) and then converted to calibrated calendar ages using the CALIB 6.1.1 program (Reimer et al., 2009). Additional age control was provided by diatom and radiolarian biostratigraphy. For radiolarian analysis, freeze-dried samples (0.4–1 g) were weighed and then wet-sieved (45- $\mu$ m mesh size). Opal particles were extracted from the residue using the elutriation method (Itaki, 2006) and then mounted in Canada Balsam. Radiolarian skeletons were observed under an optical microscope at magnifications of 100 $\times$  and 400 $\times$ . Cyclic variations in MS values, grain size, and sediment facies were used to identify glacial and interglacial stages.

Forty bulk sediment aliquots were washed and treated with a 5% hydrogen peroxide and 35% HCl solution to remove organic matter and carbonate. The samples were washed five times and sieved through a 63- $\mu$ m mesh for removal of sand- and gravel-sized grains. Sr and Nd isotope analyses, including chemical separation and multi-collector thermal ionization mass spectrometry, were performed at the Korea Basic Science Institute (KBSI). The <63- $\mu$ m fraction was dissolved with a mixed acid of HF + HClO<sub>4</sub>(10:1) for 24 h in a tightly closed Teflon vial at 120°C on a hot plate. Sr and rare earths were separated using conventional cation exchange column chemistry (Dowex AG50W-X8, #200–400, H<sup>+</sup> form) using HCl media. Nd was separated by the second-step cation exchange column chemistry using 2-ethylhexyl phosphoric acid (HDEHP)-coated Teflon powder with HCl media, and loaded on Re filament with 0.1 M H<sub>3</sub>PO<sub>4</sub>. Sr and Nd isotope ratios were measured by a multi-collector thermal ionization mass spectrometer (VG54-30, Isoprobe-T) equipped with nine faraday cups. Measurement of Sr and Nd was performed in dynamic mode.  $^{87}\text{Sr}/^{86}\text{Sr}$  and  $^{143}\text{Nd}/^{144}\text{Nd}$  ratios were corrected for instrumental fractionation using  $^{87}\text{Sr}/^{86}\text{Sr} = 0.1194$  and  $^{146}\text{Nd}/^{144}\text{Nd} = 0.7219$ , respectively. Replicate analyses of the NBS987 and La Jolla standard gave means of  $^{87}\text{Sr}/^{86}\text{Sr} = 0.710249 \pm 0.000004$  ( $n = 30$ ,  $2\sigma$  SE) and  $^{143}\text{Nd}/^{144}\text{Nd} = 0.511826 \pm 0.000006$  ( $n = 30$ ,  $2\sigma$  SE). Total procedural blank levels were less than 0.1 ng for Sr and 30 pg for Nd. The

concentrations of trace and rare earth elements (REE) were analyzed by an inductively coupled plasma mass spectrometer (model VG PQ III) at the Korea Polar Research Institute. The sample preparation and analytical procedures followed those described by Hur et al. (2003). To complement the chemical characteristics identified from fine-grained sediment, sand-sized grains were separated from 15 sand-rich (>10 wt.%) sediment samples, and quartz grains were point-counted (about 250 counts) under a polarized microscope.

## Results

### Magnetic susceptibility and grain size

Most sediments of core GC05-DP02 consist of grayish fine-grained sediment, with more than 90% silt- and clay-sized particles in most subsamples (Fig. 2). Down-core variation in color and type of sediment generally coincides with variations in MS and grain size (Fig. 2). Low-MS intervals are characterized by finer-grained sediments with either bioturbations or laminations, whereas high-MS intervals are mostly composed of coarser-grained, structureless sandy mud (Fig. 2). Clasts (>2 mm in diameter) are rarely found in low-MS intervals, but a few intermediate to mafic volcanic and plutonic clasts (up to 3 cm in diameter) were observed in high-MS intervals. Sediment with more than 8–10 wt% sand generally shows high MS values, but thin sand-rich layers in finer-grained intervals (e.g., layers at about 1-m and 3-m depths) do not accompany high MS values (Fig. 2).

### Age determination

We could not measure a continuous foraminiferal  $\delta^{18}\text{O}$  curve because of poor carbonate preservation except for the two uppermost high-MS intervals (19–73 cm and 148–187 cm). AMS  $^{14}\text{C}$  dates of the three planktonic foraminiferan samples from the uppermost high-MS interval indicate its deposition during the last glacial period:  $25.8 \pm 0.2$   $^{14}\text{C}$  ka BP for the 32-cm sample,  $27.5 \pm 0.2$   $^{14}\text{C}$  ka BP for the 48-cm sample, and  $48.0 \pm 1.7$   $^{14}\text{C}$  ka BP for the 64-cm sample (Fig. 2). Calibrated ages are  $29.6 \pm 0.2$  ka BP for the sample from 32 cm and  $31.1 \pm 0.1$  ka BP for the sample from 48 cm, respectively. We used uncalibrated radiocarbon ages for the calculation of sedimentation rates because radiocarbon age for the 64-cm sample is beyond the range of valid radiocarbon ages for CALIB 6.1.1 program (Reimer et al., 2009). Sedimentation rates between 32- and 48-cm depth ranges from 7.7 to 11 cm/ $^{14}\text{C}$  ka, and the rate between 48 and 64 cm ranges from 0.71 to 0.86 cm/ $^{14}\text{C}$  ka. This indicates that the sedimentation rate was not constant and implies that there might have been episodes of erosion and/or non-deposition which are not evident in the physical stratigraphic record. In the studied core the last-abundant-appearance datum of the diatom *Hemidiscus karstenii* lies between 180 and 190 cm, which represents a depositional age of approximately 190 ka (Burckle and Burak, 1988; Gersonde and Barcéna, 1998). This datum is correlated with the Marine Oxygen Isotope Stage (MIS) 7/6 boundary at 189.61 ka (Martinson et al., 1987). We assigned the MIS 7/6 boundary at 187 cm, where a change in sediment facies from light brownish gray mud to olive gray mud and sandy mud occurs (Fig. 2). The last occurrence of the radiolarian *Stylatractus universus* Hays at the 440 cm depth horizon indicates a depositional age of 0.42 Ma for that level (i.e., Lazarus, 1992; McIntyre and Kaczmarzka, 1996), and it is correlated with the MIS 12/11 boundary at ~425 ka (Hays et al., 1976) and Glacial Termination V at 424 ka (Lisiecki and Raymo, 2005).

The radiocarbon dates and correlation of MS with the identified MIS boundaries (7/6 and 12/11) suggest that the MS variation was controlled by glacial–interglacial cycles. The high-MS and low-MS intervals represent deposition during glacial and interglacial periods, respectively. MIS boundaries that were not constrained by radiocarbon dating or siliceous biostratigraphy were identified on the basis of changes in MS value and sediment facies (Fig. 2).

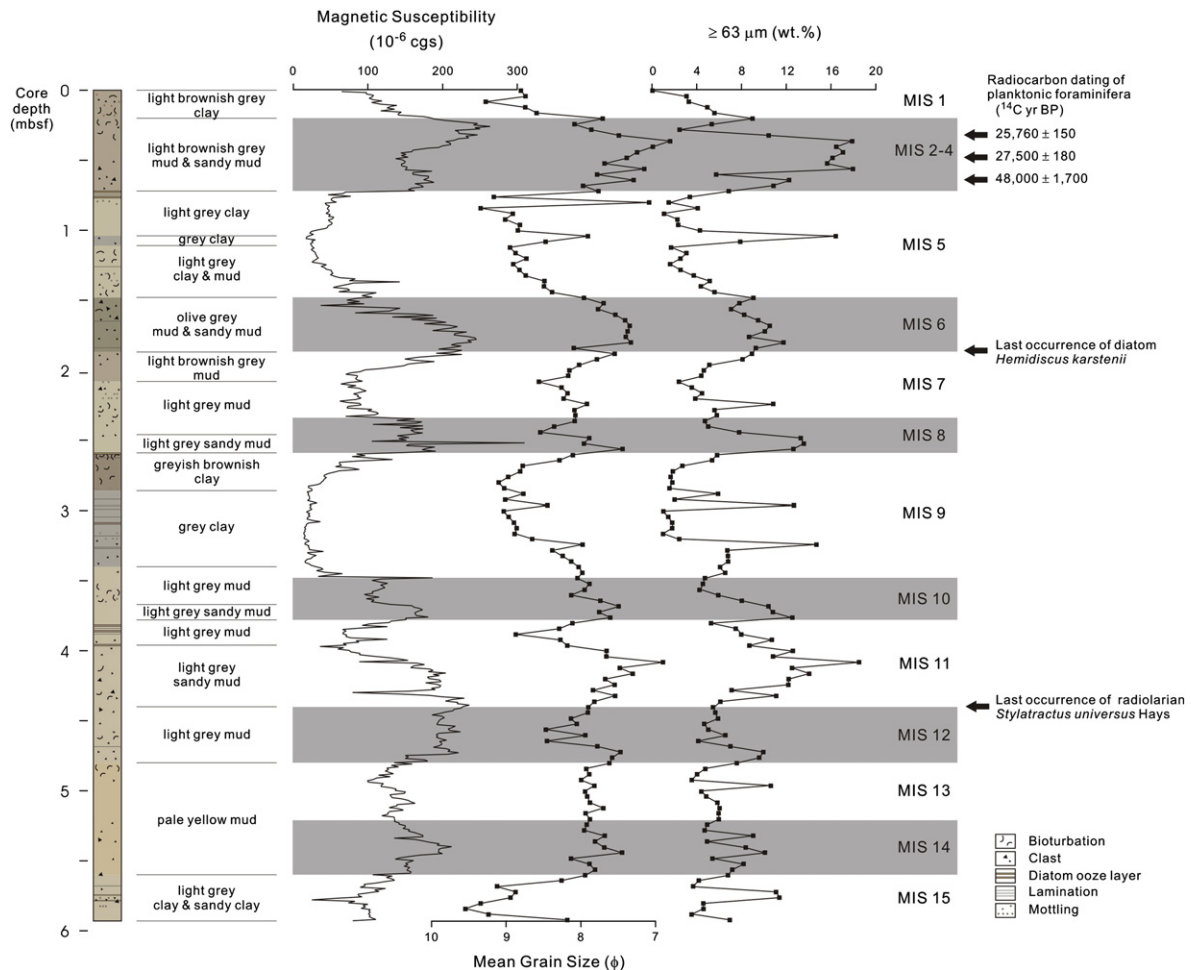


**Figure 2.** Down-core variations in sediment facies, magnetic susceptibility (MS), mean grain size, and wt.% of sand- and gravel-sized grains of core GC05-DP02.

### Trace and rare earth elements

Rare earth element (REE) distribution in the core sediments (Table 1) was plotted against the North American shale composite (NASC) (Fig. 3). Compared with the NASC, the southern Drake Passage sediments are characterized by lower concentrations of REE, with more depleted light REE than heavy REE (lower  $La_N/Sm_N$ ), and a more positive Eu anomaly ( $Eu^*$ ). The Eu anomaly was calculated by comparing the measured concentration of Eu with a geometric mean of the Sm and Gd concentrations (Taylor and McLennan, 1985). The more depleted light REE over heavy REE ratio and more positive Eu anomaly suggest that source rocks were less fractionated than upper crustal rocks. Both glacial sediments and interglacial sediments show similar REE abundances and distribution patterns (Fig. 3A). An exception is the MIS 5 sediment sample from the 120-cm depth interval, which shows a REE distribution pattern similar to that of the NASC. The glacial and interglacial sediments were plotted on a La–Th–Sc discrimination plot (Fig. 3B) to discriminate the tectonic setting of the source rocks (Bhatia and Crook, 1986; Cullers, 1994). The diagram shows that the core sediments are comparable with greywackes derived from oceanic and continental island arcs (Fig. 3B), and their high Sc ratio suggests sediment contribution from mafic source rocks (Cullers, 1994). Glacial sediments are more homogeneous than interglacial sediments in terms of trace element composition, and some interglacial sediments have distinctively lower Sc ratio (Fig. 3B), indicating sediment influx from more felsic sources (Fig. 3B). Down-core variations in the Eu anomaly, the chondrite-normalized La/Sm ratio, and the Th/Sc ratio show cyclic variations according to the glacial-interglacial cycle except MIS 7 (Fig. 4). A more prominent negative

Eu anomaly and higher La/Sm and Th/Sc ratios during interglaciations, especially MIS 5, suggest sediment supply from more fractionated source rocks (Fig. 4).

### Nd and Sr isotopes

The  $\epsilon_{Nd}$  value for the samples analyzed ranges from  $-8.68$  to  $-2.59$  with a mean of  $-4.43$ , and the  $^{87}Sr/^{86}Sr$  ratio ranges from 0.7067 to 0.7165 with a mean of 0.7085 (Table 2). Down-core variations in  $\epsilon_{Nd}$  and  $^{87}Sr/^{86}Sr$  of the core clearly show the control of glacial cycles on the Nd and Sr isotopic compositions (Fig. 4). Interglacial sediments tend to have lower  $\epsilon_{Nd}$  values (mean  $-4.97$ ) and higher  $^{87}Sr/^{86}Sr$  ratios (mean: 0.7094) than glacial sediments (mean  $\epsilon_{Nd}$ :  $-3.69$ ; mean  $^{87}Sr/^{86}Sr$ : 0.7073). The Nd and Sr isotopic composition of MIS 7 sediments deviate from this general trend, showing similar  $\epsilon_{Nd}$  values and a slightly increased  $^{87}Sr/^{86}Sr$  ratio relative to glacial sediments (Fig. 4). MIS 5 sediments show the lowest  $\epsilon_{Nd}$  and the highest  $^{87}Sr/^{86}Sr$  ratio since MIS 15.  $\epsilon_{Nd}$  values tend to gradually decrease and  $^{87}Sr/^{86}Sr$  ratios increase during successive interglacial periods except for MIS 7 (Fig. 4). In contrast, the Nd and Sr isotopic composition of glacial sediments shows little variation during glacial periods. It is also noted that the  $\epsilon_{Nd}$  values and  $^{87}Sr/^{86}Sr$  ratios for glacial sediments from different isotopic stages are similar to each other (Fig. 4).

### Sand petrography

Quartz content of sand-sized grains in the analyzed sand-rich sediments ranges from 31 to 51%. Down-core variation in quartz abundance shows that the quartz content of interglacial sediments is

**Table 1**  
Composition of trace and rare earth elements of sediment samples from core GC05-DP02. Concentrations in ppm.

Depth below seafloor (cm)	Ce	Dy	Er	Eu	Gd	Ho	La	Lu	Nd	Pr	Sm	Sc	Tb	Th	Tm	U	Yb	Y	Mo	Nb	Zr	Ba
1	35.51	3.21	2.08	0.90	3.38	0.67	16.50	0.32	16.24	4.03	3.18	17.74	0.52	5.68	0.31	1.62	2.07	16.68	0.76	9.69	123.40	440.31
10	37.27	3.35	2.18	0.97	3.47	0.70	17.06	0.33	16.93	4.26	3.32	16.90	0.55	5.48	0.31	1.63	2.15	16.99	0.66	7.71	125.71	446.46
20	39.01	3.75	2.38	1.09	3.84	0.78	18.15	0.35	18.38	4.55	3.68	17.29	0.61	5.19	0.34	1.55	2.29	18.45	0.29	5.33	97.36	457.27
25	40.33	3.78	2.34	1.10	4.02	0.76	18.64	0.35	19.01	4.70	3.79	17.19	0.62	5.51	0.34	1.49	2.31	18.27	0.58	8.28	97.24	406.72
45	38.33	3.36	2.08	0.99	3.58	0.68	17.35	0.32	17.44	4.38	3.45	13.73	0.55	5.48	0.30	1.51	2.06	15.88	0.44	6.98	106.34	406.63
50	40.50	3.58	2.26	1.05	3.87	0.72	18.89	0.34	18.67	4.69	3.67	15.55	0.59	5.70	0.33	1.63	2.20	17.17	0.48	8.76	109.55	449.00
60	40.29	3.60	2.26	1.05	3.86	0.73	18.89	0.34	18.52	4.65	3.67	15.93	0.59	5.49	0.33	1.56	2.18	17.04	0.38	6.70	106.02	438.44
70	37.57	3.51	2.22	1.03	3.75	0.72	17.51	0.33	17.54	4.36	3.56	16.43	0.58	5.21	0.32	1.42	2.12	16.38	0.52	6.27	107.36	405.18
80	41.55	3.29	2.11	0.91	3.60	0.67	19.30	0.33	18.45	4.71	3.45	11.55	0.53	6.72	0.31	1.88	2.09	14.21	0.41	11.54	137.00	527.71
95	45.74	3.58	2.29	0.99	3.99	0.72	21.68	0.35	20.30	5.21	3.79	14.42	0.60	7.55	0.34	1.92	2.30	15.64	0.30	11.13	123.13	541.71
105	38.02	3.13	2.09	0.81	3.32	0.65	16.87	0.34	16.81	4.30	3.13	10.50	0.50	7.27	0.31	1.97	2.16	13.03	0.43	14.04	177.38	574.74
120	81.21	5.10	3.18	1.18	5.85	1.02	34.46	0.48	30.79	8.11	5.53	12.36	0.86	9.12	0.45	2.49	3.10	21.20	1.19	31.78	242.35	463.17
140	41.32	3.80	2.44	1.07	4.01	0.78	18.51	0.38	18.99	4.76	3.74	16.36	0.61	7.38	0.36	1.91	2.48	16.01	1.53	11.17	126.96	525.70
160	40.57	3.74	2.40	1.09	4.05	0.77	18.92	0.36	18.91	4.72	3.75	15.61	0.61	6.38	0.35	1.56	2.33	16.09	0.30	8.13	99.51	443.60
180	44.35	4.20	2.62	1.24	4.55	0.85	20.67	0.39	21.15	5.21	4.26	17.17	0.69	6.37	0.38	1.70	2.57	18.07	0.57	7.11	107.23	473.47
195	42.05	3.90	2.44	1.16	4.24	0.78	19.70	0.36	19.88	4.91	3.92	16.28	0.63	6.21	0.35	1.67	2.36	16.48	0.52	7.90	111.63	476.67
205	35.06	3.36	2.17	0.96	3.55	0.69	16.56	0.33	16.42	4.08	3.28	14.75	0.54	5.47	0.32	1.50	2.14	14.51	0.64	7.47	104.12	443.89
215	37.35	3.51	2.28	0.99	3.72	0.73	17.53	0.35	17.29	4.34	3.43	13.63	0.57	5.48	0.33	1.65	2.24	14.93	0.42	7.94	114.47	458.02
230	41.01	3.84	2.42	1.10	4.09	0.77	19.10	0.36	19.19	4.78	3.79	15.77	0.63	6.09	0.35	1.60	2.33	15.88	0.29	5.60	104.67	477.63
250	43.71	3.79	2.42	1.13	4.22	0.77	20.24	0.36	20.07	5.05	3.92	14.77	0.63	6.56	0.35	1.75	2.39	15.42	0.41	8.06	100.69	495.33
260	45.41	3.94	2.50	1.17	4.34	0.81	20.98	0.38	20.75	5.22	4.05	15.32	0.65	6.83	0.37	1.84	2.49	16.14	0.36	8.26	112.18	517.99
280	47.52	3.79	2.44	1.07	4.18	0.78	22.68	0.37	21.33	5.44	3.99	14.43	0.63	7.59	0.37	2.08	2.42	15.90	0.37	6.58	117.76	544.24
300	48.10	3.96	2.57	1.11	4.38	0.81	22.37	0.40	21.63	5.48	4.13	16.37	0.65	8.11	0.38	2.17	2.55	15.96	0.32	7.52	117.44	584.41
320	40.24	3.45	2.25	1.00	3.69	0.72	18.28	0.35	17.74	4.50	3.45	14.81	0.57	6.31	0.33	1.88	2.24	14.14	0.77	8.38	104.08	505.55
340	44.52	4.05	2.56	1.14	4.32	0.82	20.62	0.39	20.42	5.14	4.05	15.48	0.66	7.08	0.37	1.92	2.50	16.30	0.44	4.31	104.22	502.35
350	39.96	3.84	2.43	1.11	4.11	0.79	18.57	0.36	18.90	4.70	3.79	15.04	0.63	5.69	0.35	1.62	2.36	15.61	0.38	8.09	86.43	464.12
370	41.00	3.79	2.40	1.13	4.14	0.78	19.16	0.36	19.22	4.78	3.80	15.72	0.63	6.25	0.35	1.62	2.34	15.60	0.35	7.57	102.49	470.43
385	34.47	3.40	2.20	0.97	3.67	0.70	18.01	0.34	17.97	4.50	3.43	8.73	0.55	6.53	0.32	1.66	2.18	12.93	0.39	9.40	116.52	515.78
395	45.74	3.81	2.42	1.09	4.19	0.77	21.20	0.37	20.32	5.16	3.92	15.17	0.62	7.69	0.35	1.95	2.38	14.84	0.79	7.36	103.90	522.05
405	46.17	4.01	2.51	1.16	4.37	0.81	21.43	0.39	20.95	5.27	4.09	14.73	0.66	6.95	0.37	1.96	2.49	15.88	0.45	8.86	108.53	518.11
420	41.97	3.88	2.54	1.10	4.11	0.80	19.47	0.39	19.21	4.83	3.80	14.00	0.63	7.07	0.37	2.04	2.55	15.27	1.82	6.57	128.32	524.91
440	39.27	3.79	2.37	1.12	4.12	0.77	18.32	0.35	18.67	4.60	3.82	14.26	0.63	5.49	0.35	1.48	2.35	14.65	0.39	4.51	82.13	448.65
460	42.78	3.96	2.49	1.15	4.35	0.81	20.10	0.37	20.00	4.98	4.00	15.89	0.65	6.20	0.36	1.63	2.45	15.82	0.38	8.01	94.18	485.43
480	40.39	4.17	2.64	1.23	4.44	0.85	18.90	0.39	19.59	4.77	4.02	17.28	0.68	5.88	0.38	1.57	2.51	16.24	0.36	5.21	103.03	481.88
500	40.41	3.81	2.43	1.12	4.13	0.78	18.94	0.37	18.99	4.73	3.73	14.64	0.63	6.23	0.35	1.65	2.38	14.76	0.35	8.63	115.03	494.22
520	42.04	4.12	2.57	1.20	4.36	0.84	19.54	0.38	19.95	4.89	4.00	16.50	0.67	6.25	0.38	1.70	2.52	15.73	0.41	6.59	105.60	498.30
540	43.37	4.14	2.58	1.23	4.44	0.84	19.86	0.39	20.53	5.05	4.10	14.74	0.68	6.47	0.38	1.69	2.58	15.19	0.40	8.63	101.69	505.53
560	40.46	4.20	2.64	1.22	4.35	0.85	18.94	0.40	19.45	4.76	3.93	17.03	0.68	5.98	0.38	1.69	2.56	16.12	0.41	6.90	114.10	489.02
575	46.93	4.15	2.62	1.20	4.53	0.85	22.14	0.39	21.56	5.41	4.21	15.83	0.68	6.94	0.38	1.81	2.54	16.03	0.51	8.67	90.04	517.34
590	44.62	3.97	2.58	1.12	4.33	0.82	20.95	0.40	20.11	5.07	3.89	14.67	0.66	7.07	0.38	2.05	2.62	14.96	0.47	9.39	112.70	526.15

generally higher than that of glacial sediments (Fig. 4). Thin sand-rich layers at about 1 m and 3 m depths (MIS 5 and 9, respectively) have comparable sand content to glacial sediments (Fig. 2), but microscopic observation revealed that they differ from glacial sediments in that they contain much more quartz. X-radiographic and petrographic observations show that these interglacial sand-rich layers do not contain grains larger than 2 mm as are found in the glacial sediments, and it excludes ice-rafting as the main transport mechanism for the interglacial sands.

**Discussion**

*Effect of glacial–interglacial cycles on the deposition and chemistry of the late Quaternary sediments from the southern Drake Passage*

Age determination of the core shows that the variations in sediment facies and MS of the southern Drake Passage sediment are closely linked to the glacial–interglacial cycle of the late Pleistocene. Interglacial sediments are mostly composed of bioturbated or laminated clay and

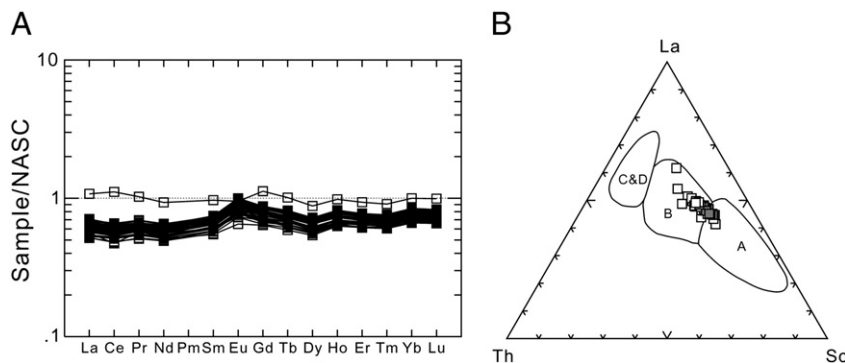


**Figure 3.** (A) Rare-earth element distribution of core GC05-DP02 sediments compared with North American Shale Composite (NASC; Gromet et al., 1984). (B) La–Th–Sc discrimination diagram for the glacial (gray square) and interglacial (white square) sediments. Compositional field of graywackes from oceanic island arc (A), continental island arc (B), active continental margin (C), and passive margin (D) are shown for comparison (Bhatia and Crook, 1986).

mud, whereas glacial sediments consist of coarser-grained, structureless sandy mud. Yoon et al. (2009) suggested sedimentary processes responsible for the deposition of glacial and interglacial sediments in the southern Drake Passage for the last 150 ka on the basis of textural and compositional analyses. They suggested that interglacial sediments in the southern Drake Passage were deposited from pelagic settling of bioclasts, meltwater plumes, and ice-rafted detritus, while glacial sediments were transported by turbid meltwater plumes. We assume similar depositional processes for core GC05-DP02 because core GC98-06 used by Yoon et al. (2009) was collected close to the present study core location (~60 km to the east) and shows comparable variation in MS for the respective time interval.

MS values in the core sediments vary in accordance with the glacial-interglacial cycle. The MS trend is apparently well correlated with that of mean grain size, with low MS values in fine-grained intervals and high MS values in coarse-grained intervals (Fig. 2). This may be partly because fine sediments generally contain more organic matter, which produces low MS values. However, considering the very low content of total organic matter in sediments from the southern Drake Passage (<0.3 wt.%; Yoon et al., 2009), it is more likely that the large difference in MS values between glacial and interglacial sediments is due to differing content of magnetic minerals. In addition, coarse-grained layers from interglacial times (e.g., layers at about 1 m and 3 m depths) have low MS values, similar to other fine-grained interglacial sediments, but are much lower than glacial sediments of similar grain size. This finding also supports the control of mineral composition, not grain size, on MS values. Observation of MS variation suggests that minerals with lower MS values are enriched in sediments from interglacial periods, while minerals with higher MS values are enriched in glacial sediments. Petrographic results are consistent with the MS observations. The variation in the content of quartz grains in the sand-sized fraction shows increased quartz content during interglacial periods (Fig. 4), which results in lower MS values because quartz is diamagnetic. Variations in MS values and quartz content with depth indicate the control of glacial-interglacial cycles on the composition of sediment transported to the basin, with more quartz during interglacial

periods and more magnetic minerals during glacial periods. The effect of glacial cycles on the chemical composition of the sediments is best shown in the down-core variation of Nd and Sr isotopic composition (Fig. 4). This climatically induced variation in Nd isotopic composition indicates that sediment provenance differed between glacial and interglacial times because Nd isotope composition reflects the average composition of the provenance and is rarely modified through earth surface processes, such as weathering and transport (Nelson and DePaolo, 1988).

Marine surface sediments near West Antarctica (West Antarctic, Antarctic Peninsula, and part of the Ross Sea sector in Fig. 5) are characterized by high  $\epsilon_{Nd}$  values, while samples from the East Antarctic region (Weddell Sea, Dronning Maud Land, Prydz Bay, Wilkes Land, and part of the Ross Sea sector in Fig. 5) show lower  $\epsilon_{Nd}$  values due to their derivation from crust with older mantle extraction age (Roy et al., 2007). The  $\epsilon_{Nd}$  values from GC05-DP02 sediments are mostly higher than  $-6$ , indicating West Antarctica as a dominant sediment source area for both glacial and interglacial periods. However, some interglacial sediments show much lower  $\epsilon_{Nd}$  values than surface sediments from the West Antarctic region (Fig. 5). They also show geochemical characteristics of older, differentiated source rocks, such as high  $^{87}Sr/^{86}Sr$ , high  $La_N/Sm_N$ , low  $Eu^*$ , and high Th/Sc. This suggests that interglacial sediments were partly derived from East Antarctica. Sediment contribution from East Antarctica may have increased through each interglacial period except MIS 7, taking into consideration that  $\epsilon_{Nd}$  values of successive interglacial periods became more negative through time (Fig. 4).

#### Provenance of late Quaternary glacial and interglacial sediments from the southern Drake Passage

Late Quaternary glacial sediments from the southern Drake Passage are characterized by little variation in their chemical composition (Fig. 4). This indicates that sediment provenance for glacial sediments has varied little over the last ~600 ka. The  $\epsilon_{Nd}$  values of the glacial sediments are all higher than  $-6$ , implying that West Antarctica (the

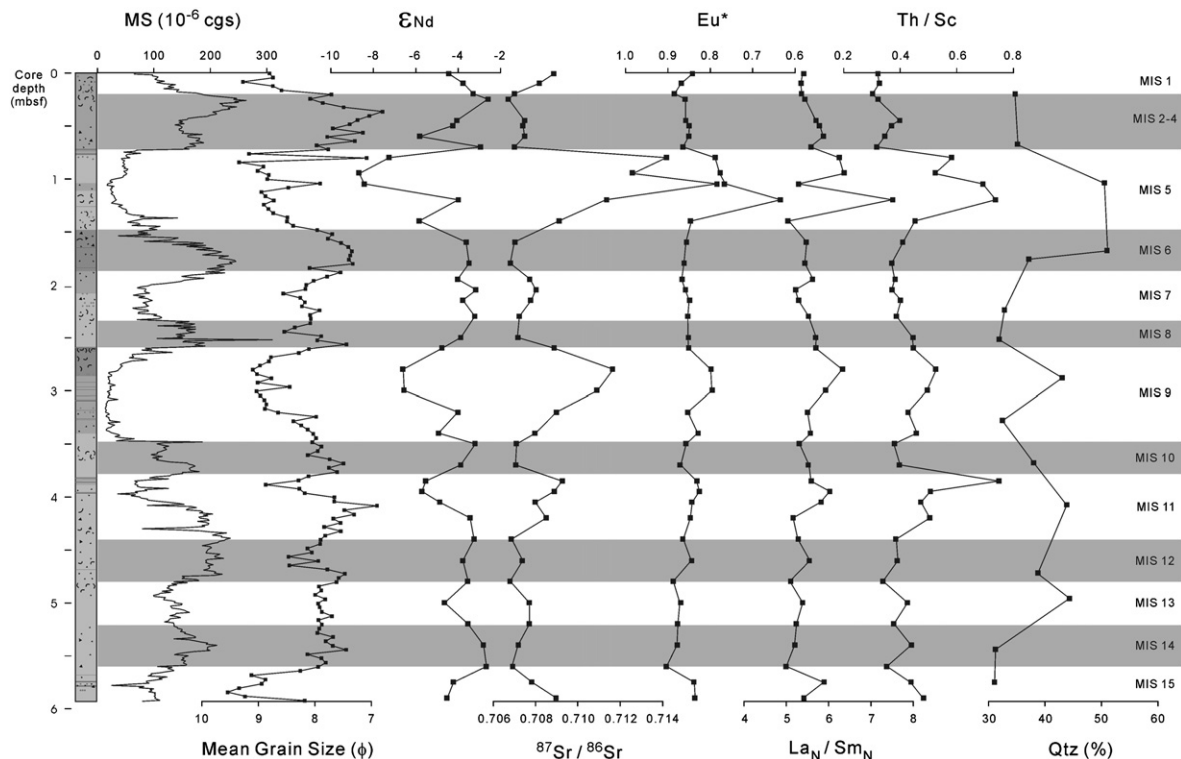


Figure 4. Downcore variations in Nd and Sr isotope composition,  $Eu^*$ ,  $La_N/Sm_N$ , Th/Sc, and quartz content of core GC05-DP02, compared to MS and mean grain size.

**Table 2**  
Nd and Sr isotopic ratios of the sediment samples from core GC05-DP02.

Depth below seafloor (cm)	<sup>143</sup> Nd/ <sup>144</sup> Nd	2σ	ε <sub>Nd</sub>	<sup>87</sup> Sr/ <sup>86</sup> Sr	2σ
1	0.512411	0.000014	-4.43	0.708847	0.000017
10	0.512445	0.000013	-3.76	0.708170	0.000012
20	0.512469	0.000014	-3.30	0.707034	0.000012
25	0.512505	0.000017	-2.59	0.706705	0.000011
45	0.512430	0.000014	-4.06	0.707477	0.000012
50	0.512420	0.000012	-4.25	0.707412	0.000014
60	0.512340	0.000018	-5.81	0.707489	0.000010
70	0.512487	0.000014	-2.95	0.707012	0.000024
80	0.512266	0.000013	-7.26	0.714178	0.000010
95	0.512193	0.000016	-8.68	0.712567	0.000010
105	0.512205	0.000014	-8.45	0.716544	0.000013
120	0.512433	0.000019	-4.00	0.711342	0.000014
140	0.512339	0.000030	-5.83	0.709100	0.000011
160	0.512452	0.000015	-3.63	0.707013	0.000015
180	0.512459	0.000017	-3.49	0.706792	0.000019
195	0.512431	0.000011	-4.04	0.707732	0.000011
205	0.512476	0.000034	-3.16	0.708014	0.000011
215	0.512444	0.000016	-3.78	0.707785	0.000014
230	0.512473	0.000015	-3.22	0.707230	0.000012
250	0.512439	0.000013	-3.88	0.707165	0.000011
260	0.512394	0.000013	-4.76	0.708897	0.000011
280	0.512299	0.000012	-6.61	0.711662	0.000011
300	0.512302	0.000015	-6.55	0.710917	0.000011
320	0.512432	0.000012	-4.02	0.708993	0.000010
340	0.512385	0.000013	-4.94	0.707968	0.000011
350	0.512474	0.000014	-3.20	0.707092	0.000010
370	0.512439	0.000013	-3.88	0.707064	0.000011
385	0.512354	0.000015	-5.54	0.709256	0.000013
395	0.512345	0.000021	-5.72	0.708894	0.000013
405	0.512388	0.000015	-4.88	0.707975	0.000011
420	0.512462	0.000015	-3.43	0.708534	0.000011
440	0.512471	0.000015	-3.26	0.706871	0.000010
460	0.512444	0.000015	-3.78	0.707379	0.000011
480	0.512457	0.000015	-3.53	0.706813	0.000012
500	0.512400	0.000015	-4.64	0.707735	0.000012
520	0.512456	0.000015	-3.55	0.707717	0.000012
540	0.512494	0.000015	-2.81	0.707183	0.000012
560	0.512501	0.000015	-2.67	0.706909	0.000012
575	0.512421	0.000015	-4.23	0.707850	0.000015
590	0.512406	0.000013	-4.53	0.708971	0.000013

$\epsilon_{Nd} = [({}^{143}\text{Nd}/{}^{144}\text{Nd})_{\text{sample}} / ({}^{143}\text{Nd}/{}^{144}\text{Nd})_{\text{CHUR},0} - 1] \times 10^4$ . The value  $({}^{143}\text{Nd}/{}^{144}\text{Nd})_{\text{CHUR},0} = 0.512638$  (Wasserburg et al., 1981) was used in this study.

Antarctic Peninsula and West Antarctic sectors) was the source region during glacial periods (Fig. 5). The AP sector is more likely the main source region considering the core location and the glacial extent during glacial periods. During the last glacial maximum (LGM), the northern AP and the SSI were covered by a grounded ice sheet that extended near the shelf break (Larter and Barker, 1991; Heroy and Anderson, 2005). The advance of the ice sheet would have provided a condition conducive for sediments from the AP reaching the core location. Glacial terrigenous mud in the southern Drake Passage was deposited from sediment-laden meltwater plumes generated at the front of the grounded ice sheet (Yoon et al., 2009). To the southeast of the SSI, the ice sheet was separated from the northern AP by the Bransfield Strait during the LGM, and glacial sediments from the northern AP were deposited in the Bransfield Strait (Heroy and Anderson, 2005). This excludes the northern AP as the possible source area for the LGM sediment near the South Shetland Trench. Lee et al. (2005) analyzed major, trace, and REE chemistry of near-surface sediments from the Bransfield Basin, and suggested that the north-western Bransfield sediments were mainly derived from the SSI whereas southeastern Bransfield sediments were derived from the northern Antarctic Peninsula. The trace element distribution of the glacial sediments shows a similar pattern to that of the northwestern Bransfield sediments (Fig. 6). Therefore, the SSI seems to be the main sediment source region for the glacial sediments. It is noted that part of the glacial sediments could have been derived from other areas of

the AP and West Antarctic sectors, although the contribution would have been minor.

During glaciations, older shelf sediments were also a potential sediment source because they could be reworked by the grounding of the ice sheets. The increased content of extinct diatoms in glacial sediments from the southern Drake Passage (Yoon et al., 2009) confirms the reworking of older shelf sediments. Despite sediment input from reworked sediments, the glacial sediments in the southern Drake Passage still show similar chemical composition to the SSI-derived sediments. This implies that either (1) the chemical composition of the reworked shelf sediments cannot be distinguished from the SSI-derived sediments, which is more likely considering the proximity to the SSI, or (2) if the shelf sediments have a different composition from the SSI-derived sediments, the contribution of the shelf sediments to the glacial sediments in the southern Drake Passage would have been minor.

Detrital sediments deposited during interglacial periods in the southern Drake Passage are composed of sediments derived from West Antarctica and East Antarctica. The interglacial sediments are a mixture of various source regions, so we could not identify West Antarctic provenance in more detail as we have done for glacial sediments. The SSI and northern AP regions seem the most probable candidates for West Antarctic provenance considering their proximity to the core location. On the other hand, East Antarctic-derived sediment should be transported from outside the basin, from the Ross Sea sector or farther west via the ACC and/or from the Weddell Sea sector via currents from the Weddell Sea.

The core location (water depth 3503 m) is under the influence of the ACC to a depth of more than 2500 m (i.e., Nowlin and Zenk, 1988), so suspended sediment and ice-rafted detritus can be transported from the west via the CDW and surface water of the ACC. However, for detritus from the Ross Sea sector or farther west to be deposited at the core location, a transport distance of more than 5000 km would be required. At present, most icebergs from East Antarctica drift westward in a westward-flowing surface current around the Antarctic coast and few icebergs are deflected north and entrained in the eastward-flowing ACC (Williams et al., 2010, and references therein). As a result, present-day surface sediments in the Southern Ocean contain ice-rafted detritus from nearby source areas. Nd and Sr isotopes in the fine fraction and <sup>40</sup>Ar/<sup>39</sup>Ar ages of hornblende grains of Antarctic surface sediment samples are comparable to geochemical characteristics of rock outcrops proximal to sampling sites (Hemming et al., 2007; Roy et al., 2007), also indicating that modern Antarctic sediments are not transported far from their sources.

Chemical composition of the core sediments indicates that sediment input from East Antarctica has increased during the Holocene. If detritus of lower  $\epsilon_{Nd}$  values from East Antarctica was transported from the west, the  $\epsilon_{Nd}$  value of the core surface sediment would be similar to or higher than that of surface sediments to the west. Furthermore, since the core site is close to the northern AP, where the surface sediments show the highest  $\epsilon_{Nd}$  values (7, 8, 16 in Fig. 7; Table 3), it is expected that input from the northern AP region will cause an increase in the  $\epsilon_{Nd}$  values of the core surface sediment. The combined effect of a western source of lower  $\epsilon_{Nd}$  values and high  $\epsilon_{Nd}$  values from northern AP-derived sediments would make the  $\epsilon_{Nd}$  values of the core surface sediment higher than those of sediments to the west. However, surface sediment from core GC05-DP02 (1 in Fig. 7) has lower  $\epsilon_{Nd}$  values than surface sediments west of the study area (13 and 14 in Fig. 7). It does not seem likely that detritus of lower  $\epsilon_{Nd}$  values was transported from the west via the ACC.

Surface sediments from the Weddell Sea and Powell Basin have much lower  $\epsilon_{Nd}$  values than those from the AP region (Fig. 7); thus sediment input from the Weddell Sea during interglacials could make the  $\epsilon_{Nd}$  value of the core sediment lower than that of glacial sediments. In the southern Scotia Sea, geochemical and mineralogical composition of late Quaternary sediments also varies with glacial-interglacial cycles (Diekmann et al., 2000; Walter et al., 2000). As in the southern Drake

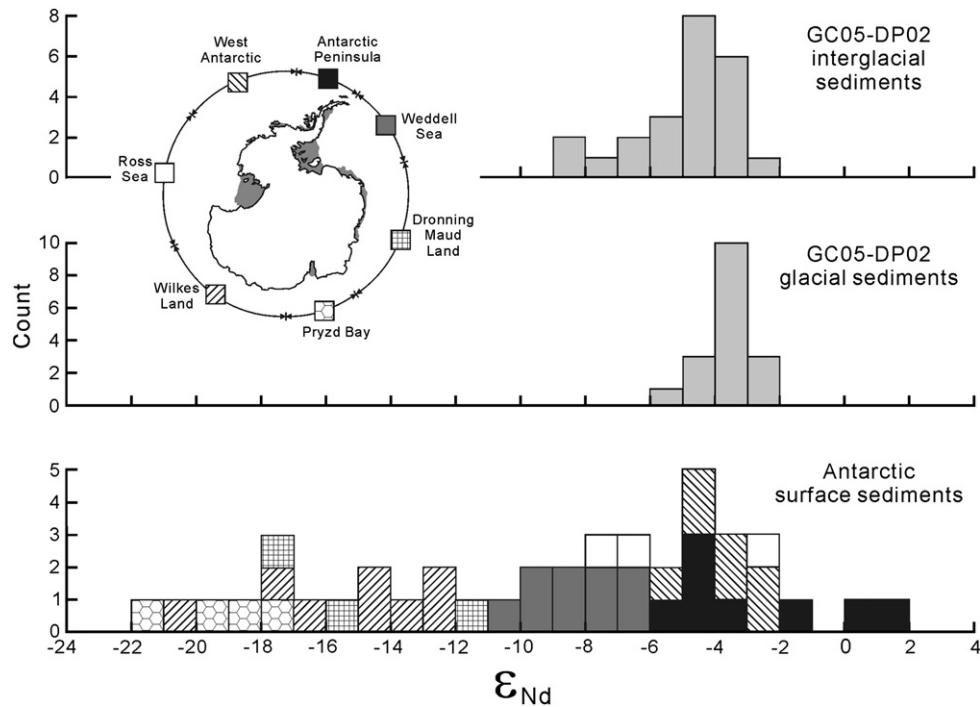


Figure 5.  $\epsilon_{Nd}$  values of glacial and interglacial sediments of core GC05-DP02 and marine surface-sediment samples around Antarctica (Roy et al., 2007).

Passage, input of more basic, undifferentiated, and young materials with high  $\epsilon_{Nd}$  values ( $>-4$ ) increased during glacial periods (Diekmann et al., 2000; Walter et al., 2000). During interglacial periods, sediments in the southern Scotia Sea are characterized by low  $\epsilon_{Nd}$  values ( $<-8$ ), indicative of an increased contribution of detritus from East Antarctica (Walter et al., 2000). It was suggested that Weddell Sea Bottom Water played a major role in supplying the interglacial sediments of East Antarctic origin to the southern Scotia Sea (Walter et al., 2000). Comparison of the geochemical characteristics of sediments from the Weddell Sea and the southern Scotia Sea suggests the Weddell Sea region as a possible East Antarctic source for the interglacial sediments from the southern Drake Passage.

#### Paleoceanographic and paleoclimatic implications

The surface current around the northern AP flows in a complicated pattern but includes currents flowing westward along the southern

margin of the Bransfield Strait (Hofmann et al., 1996; Fig. 1). It would be possible for detritus from the Weddell Sea to reach the core location as ice-rafts if icebergs are transported via this current to the northwestern side of the AP and then deflected to the north and entrained into the ACC. The presence of ice-rafted detritus layers during the last interglacial periods from the southern Drake Passage (Yoon et al., 2009) implies that ice rafting might have occurred during the peaks of some past interglaciations. However, the chemistry of the near-surface sediments from the Bransfield Strait indicates the SSI and AP as the sources, with no indication for older, differentiated sources (Lee et al., 2005). This suggests that sediment input from the Weddell Sea region transported by surface currents to the core location would be modest at present. It is more likely that the core location was affected by a deep-water flow from the Weddell Sea during interglacial periods. The subordinate role of ice rafts in sediment transport during interglacial periods is supported by the minor amount of coarse particles larger than  $63\ \mu\text{m}$  (generally  $<5\%$ ) and rare clasts in interglacial sediments from the southern Drake Passage (Fig. 2). The occurrence of drift deposits associated with deep- and bottom-currents in the northwestern Weddell Sea during interglacial periods supports this interpretation (Gilbert et al., 1998). The northern extent of the deep-water current in the southern Drake Passage must be confirmed by more detailed oceanographic studies.

Paleoceanographic proxies imply a northward shift in the major circum-Antarctic fronts by  $5\text{--}10^\circ$  during glacial periods, although some researchers have maintained that the frontal positions during the LGM were similar to those of today and have suggested a northward shift of ecosystem rather than a frontal migration (Hemming et al., 2007, and references therein). A small northward shift ( $1\text{--}2^\circ$ ) of the SBACC was suggested by Hemming et al. (2007) based on a comparison of Sr isotope ratios from the Holocene and LGM along a transect northward from the Ross Sea. During glacial periods, the SBACC in the southern Drake Passage may either have shifted northward, as in the Ross Sea sector, or it may have remained in a similar position to that of today. Provenance analysis in this study suggests a sediment input from the Weddell Sea during interglacial periods. Therefore, it is likely that sediment from the Weddell Sea would also have reached the core location during glacial periods whether the front moved northward or

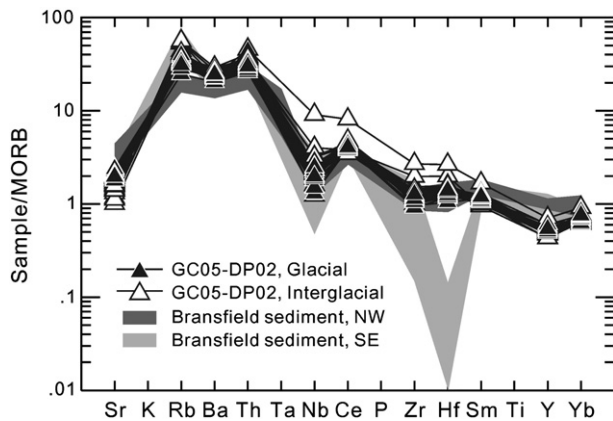


Figure 6. Trace-element concentrations of the late Quaternary glacial and interglacial sediments from the southern Drake Passage plotted on the mid-ocean ridge basalt (MORB)-normalized spider diagram of Pearce (1983). Trace element distribution of the near-surface sediments from the northwestern and southeastern Bransfield Strait is shown for comparison (Lee et al., 2005).

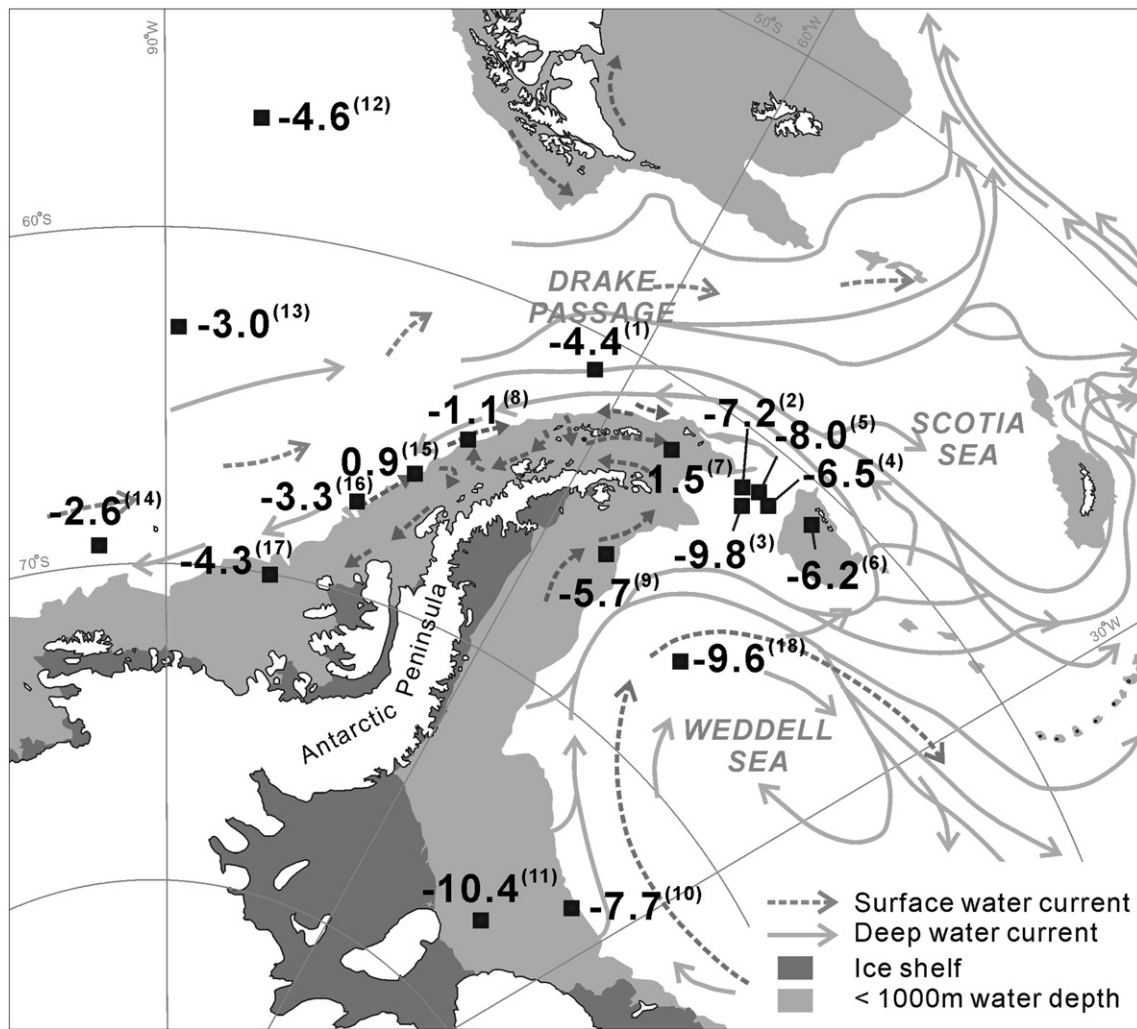


Figure 7.  $\epsilon_{Nd}$  values of surface sediments from study area. Sample location, water depth, and reference for the data are shown in Table 3.

remained in the same position, if other environmental conditions were similar to those in interglacial periods. The chemical composition of the sediments from the southern Drake Passage, however, indicates little sediment input from the Weddell Sea during glacial periods. The advance of grounded ice sheets near the shelf break during glacial periods (e.g., Larter and Barker, 1991; Heroy and Anderson, 2005) may

have been advantageous for increasing the amount of sediment from the SSI region that reached the core location, and the increase in the SSI-derived sediments may have weakened the signature of the Weddell Sea-derived sediments. It is also likely that sediment transport from the Weddell Sea decreased during glacial periods due to changes in the formation and velocity of bottom water in the Weddell Sea. Changes in

Table 3  
 $\epsilon_{Nd}$  values of surface sediments around the northern Antarctic Peninsula.

Number in Fig. 7	Sample ID	Latitude	Longitude	Water depth (m)	Depth below seafloor (cm)	$\epsilon_{Nd}$	Reference
1	GC05-DP02	61°02.7096' S	62°38.3859' W	3503	1	-4.43	This study
2	GC01-PW2	61°32'47" S	50°31'26" W	3144	0	-7.25	This study
3	GC01-PW3	62°10'30" S	49°35'38" W	3335	0	-9.76	This study
4	BC03-PW02	61°06.452' S	48°54.277' W	1882	0	-6.47	This study
5	GC04-G03	61°19.338' S	49°48.053' W	2907	0	-8.02	This study
6	D-ORC-15	61°95.0' S	45°42.1' W	290	1	-6.2	Walter et al., 2000
7	PS1537-2	61°59.0' S	55° 52.0' W	1812	1	1.5	Walter et al., 2000
8	PS1563-1	64°46.9' S	68°27.3' W	2800	1	-1.1	Walter et al., 2000
9	PS2805-1	66°05.2' S	56°31.9' W	466	1	-5.7	Walter et al., 2000
10	PS1490-2	74°40.7' S	35°05.0' W	497	1	-7.7	Walter et al., 2000
11	PS1016-1	77°15.3' S	40°50.0' W	702	0.3	-10.4	Walter et al., 2000
12	PS2716-2	56°01.2' S	84°54.3' W	5277	1.5	-4.6	Walter et al., 2000
13	PS2697-1	62°59.8' S	89°29.6' W	4783	1	-3.0	Walter et al., 2000
14	PS2684-1	69°25.0' S	95°01.4' W	4229	1	-2.6	Walter et al., 2000
15	ELT05-22	65.95° S	70.25° W	373		0.9	Roy et al., 2007
16	ELT05-20	67.18° S	74.78° W	2926		-3.3	Roy et al., 2007
17	ELT42-09	69.99° S	80.40° W	567		-4.3	Roy et al., 2007
18	ELT07-11	66.50° S	45.62° W	4197		-9.6	van de Fliedert et al., 2007

the amount of bottom-water production in the Weddell Sea in relation to glacial-interglacial cycles is under debate, and proxy data suggest all scenarios from decreased to increased formation of bottom water in the Weddell Sea during glacials (Krueger et al., 2012, and references therein). Krueger et al. (2012) suggested a more complex glacial environment wherein the formation of Antarctic Bottom Water increased during early glacials and then decreased during full glacial conditions. We could not distinguish early glacial signatures from full glacial signatures due to low resolution, but the deficiency of Weddell Sea-derived sediments in glacial sediments supports a decreased formation of bottom water in the Weddell Sea during glaciations in general. The velocity of Antarctic Bottom Water flowing north into the Scotia Sea was inferred to be much slower than the present velocity based on sediment grain size in the northern Weddell Sea during the LGM (Pudsey, 1992). It is noted that the hydrographic situation of a weakened bottom current in the northern Weddell Sea during glacial periods and a consequent decrease in sediment supply from the Weddell Sea is consistent with the glacial records from the southern Drake Passage.

We compared the variations in Nd and Sr isotope isotopes (Fig. 4) with the patterns of interglacial warmth recorded in the Antarctic ice core to identify the relationship between the relative amount of the Weddell Sea component in the Drake Passage sediment and the late Quaternary interglacial intensities. Ice cores from West Antarctica record only the last glacial cycle (Hammer et al., 1994; Nereson et al., 1996; Blunier and Brook, 2001), so we used the EPICA Dome C record for comparison. Paleotemperature reconstruction from the EPICA Dome C ice core indicates that “early” (800–400 ka) interglaciations showed less pronounced warmth than “late” (400–0 ka) ones (Jouzel et al., 2007; Masson-Delmotte et al., 2010). The ice-core record also indicates that MIS 5.5 was the warmest interglaciation, followed by MIS 11 and 9 (Masson-Delmotte et al., 2010). Variation in Nd and Sr isotopes suggests that the relative amount of the Weddell component in the Drake Passage sediment gradually increased during successive interglacial periods except MIS 7 (Fig. 4). Sediment supply from the Weddell Sea was greatest during MIS 5, the warmest interglacial period of the last 800 ka, and there are noticeable changes in the Eu anomaly, La/Sm ratio, and Th/Sc ratio as well as Nd and Sr isotopes during this period (Fig. 4). Second to MIS 5, the Nd and Sr isotope signature from Weddell-derived sediment is strongest in MIS 9 and 11 (Fig. 4), the third and second warmest interglacial periods of the last 800 ka, respectively (Masson-Delmotte et al., 2010). Comparison of the geochemical data of Drake Passage sediment with the paleotemperature reconstruction from the EPICA Dome C ice core suggests that sediment supply from the Weddell Sea into the southern Drake Passage increased as the interglacial intensity increased over the last ~600 ka. Increased sediment supply from the Weddell Sea implies increased deep water production in the Weddell Sea. Comparison of the chemical compositions of interglacial sediments from the southern Drake Passage suggests that deep water production in the Weddell Sea increased with increasing interglacial intensities.

## Conclusions

Late Quaternary sediments from the southern Drake Passage clearly show the influence of glacial-interglacial cycles on sediment geochemistry. The geochemical variation reflects different sediment provenance between glacial and interglacial periods, which was caused by climatically induced variations in ocean circulation and ice-sheet extent. During glacial periods, sediments were almost exclusively derived from the South Shetland Islands and shelf sediments of the South Shetland Islands. Interglacial sediments, however, are composed of detritus from East Antarctica as well as West Antarctica. The East Antarctic source for the interglacial sediments from the southern Drake Passage was inferred to be the Weddell Sea region. Sediment input from the Weddell Sea increased as interglacial warmth increased, and the influence of deep water from the Weddell Sea subsequently increased.

During glaciations, the deep water current from the Weddell Sea weakened, resulting in the dominance of the geochemical signal from West Antarctica.

## Acknowledgments

We are grateful to the crew and scientific party of the RV *Yuzhmorgeologiya* for all their help during the gravity coring on board. We acknowledge the comments from anonymous reviewers. This research was supported by KOPRI project PP12020.

## References

- Bae, S.H., Yoon, H.I., Park, B.-K., Kim, Y., 2003. Late Quaternary stable isotope record and meltwater discharge anomaly events to the south of the Antarctic Polar Front, Drake Passage. *Geo-Marine Letters* 23, 110–116.
- Bareille, G., Grousset, F.E., Labracherie, M., Labeyrie, L.D., Petit, J.-R., 1994. Origin of detrital fluxes in the southeast Indian Ocean during the last climatic cycles. *Paleoceanography* 9, 799–819.
- Bhatia, M.R., Crook, A.W., 1986. Trace element characteristics of graywackes and tectonic setting discrimination of sedimentary basins. *Contributions to Mineralogy and Petrology* 92, 181–193.
- Blunier, T., Brook, E.J., 2001. Timing of millennial-scale climate change in Antarctica and Greenland during the Last Glacial Period. *Science* 291, 109–112.
- Burckle, L.H., Burak, R.W., 1988. Fluctuations in late Quaternary diatom abundances: stratigraphic and paleoclimatic implications from subantarctic deep sea coral. *Palaeogeography, Palaeoclimatology, Palaeoecology* 67, 147–156.
- Cullers, R.L., 1994. The controls on the major and trace element variation of shales, siltstones, and sandstones of Pennsylvanian–Permian age from uplifted continental blocks in Colorado to platform sediment in Kansas, USA. *Geochimica et Cosmochimica Acta* 58, 4955–4972.
- Diekmann, B., Kuhn, G., Rachold, V., Abelmann, A., Brathauer, U., Fütterer, D.K., Gersonde, R., Grobe, H., 2000. Terrigenous sediment supply in the Scotia Sea (Southern Ocean): response to Late Quaternary ice dynamics in Patagonia and on the Antarctic Peninsula. *Palaeogeography, Palaeoclimatology, Palaeoecology* 162, 357–387.
- Gersonde, R., Barcéna, M.A., 1998. Revision of the Upper Pliocene–Pleistocene diatom biostratigraphy for the northern belt of the Southern Ocean. *Micropaleontology* 44, 84–98.
- Gilbert, I.M., Pudsey, C.J., Murray, J.W., 1998. A sediment record of cyclic bottom-current variability from the northwest Weddell Sea. *Sedimentary Geology* 115, 185–214.
- Gordon, J.E., Harkness, D.D., 1992. Magnitude and geographic variation of the radiocarbon content in Antarctic marine life: implications for reservoir corrections in radiocarbon dating. *Quaternary Science Reviews* 11, 697–708.
- Gromet, L.P., Dymek, R.F., Haskin, L.A., Korotev, R.L., 1984. The “North American Shale Composite”: its compilation, major and trace element characteristics. *Geochimica et Cosmochimica Acta* 48, 2469–2482.
- Hammer, C.U., Clausen, H.B., Langway, C.C., 1994. Electrical conductivity method (ECM) stratigraphic dating of the Byrd Station ice core, Antarctica. *Annals of Glaciology* 20, 115–120.
- Hays, J.D., Imbrie, J., Shackleton, N.J., 1976. Variations in the Earth's orbit: pacemaker of the ice ages. *Science* 194, 1121–1132.
- Hemming, S.R., van de Fliedert, T., Goldstein, S.L., Franzese, A.M., Roy, Rm, Gastineau, G., Landrot, G., 2007. Strontium isotope tracing of terrigenous sediment dispersal in the Antarctic Circumpolar Current: implications for constraining frontal positions. *Geochemistry, Geophysics, Geosystems* 8. doi:10.1029/2006GC001441.
- Hernández-Molina, F.J., Larter, R.D., Rebesco, M., Maldonado, A., 2006. Miocene reversal of bottom water flow along the Pacific Margin of the Antarctic Peninsula: stratigraphic evidence from a contourite sedimentary tail. *Marine Geology* 228, 93–116.
- Heroy, D.C., Anderson, J.B., 2005. Ice-sheet extent of the Antarctic Peninsula region during the Last Glacial Maximum (LGM) – insights from glacial geomorphology. *Geological Society of America Bulletin* 117, 1497–1512.
- Hillenbrand, C.-D., Camerlenghi, A., Cowan, E.A., Hernández-Molina, F.J., Lucchi, R.G., Rebesco, M., Uenzelmann-Neben, G., 2008. The present and past bottom-current flow regime around the sediment drifts on the continental rise west of the Antarctic Peninsula. *Marine Geology* 255, 55–63.
- Hofmann, E.E., Klinck, J.M., Lascara, C.M., Smith, D.A., 1996. Water mass distribution and circulation west of the Antarctic Peninsula and including Bransfield Strait. In: Ross, R.M., Hofmann, E.E., Quentin, L.B. (Eds.), *Foundations for ecological research west of the Antarctic Peninsula*. : Antarctic Research Series, 70. American Geophysical Union, Washington, D.C., pp. 61–80.
- Hur, S.D., Lee, J.I., Lee, M.J., Kim, Y., 2003. Determination of rare earth elements abundance in alkaline rocks by inductively coupled plasma mass spectrometry (ICP-MS). *Ocean and Polar Research* 25, 53–62 (in Korean with English abstract).
- Itaki, T., 2006. Elutriation technique for extracting radiolarian skeletons from sandy sediments and its usefulness for faunal analysis. *Radiolaria* 24, 14–18.
- Johnsson, M.J., 1993. The system controlling the composition of clastic sediments. In: Johnsson, M.J., Basu, A. (Eds.), *Processes controlling the composition of clastic sediments*: Boulder, Colorado, Geological Society of America Special Paper, 284, pp. 1–19.

- Jouzel, J., Masson-Delmotte, V., Cattani, O., Dreyfus, G., Falourd, S., Hoffmann, G., Minster, B., Nouet, J., Barnola, J.M., Chappellaz, J., Fischer, H., Gallet, J.C., Johnsen, S., Leuenberger, M., Loulergue, L., Luethi, D., Oerter, H., Parrenin, F., Raisbeck, G., Raynaud, D., Schilt, A., Schwander, J., Selmo, E., Souchez, R., Spahni, R., Stauffer, B., Steffensen, J.P., Stenni, B., Stocker, T.F., Tison, J.L., Werner, M., Wolff, E.W., 2007. Orbital and millennial Antarctic climate variability over the past 800,000 years. *Science* 317, 793–796.
- Krueger, S., Leuschner, D.C., Ehrmann, W., Schmiedl, G., Mackensen, A., 2012. North Atlantic Deep Water and Antarctic Bottom Water variability during the last 200 ka recorded in an abyssal sediment core off South Africa. *Global and Planetary Change* 80–81, 180–189.
- Larter, R.D., Barker, P.F., 1991. Neogene interaction of tectonic and glacial processes at the Pacific margin of the Antarctic Peninsula. In: Macdonald, D.I.M. (Ed.), *Sedimentation, Tectonics, and Eustasy: Sea-Level Changes at Active Margins*. : IAS Special Publication, 12. Blackwell Scientific Publications, Oxford, pp. 165–186. International Association of Sedimentologist.
- Lazarus, D.B., 1992. Antarctic Neogene radiolarians from the Kerguelen Plateau, ODP Legs 119 and 120. In: Wise, S.W., Schlich, R. (Eds.), *Proceedings of the Ocean Drilling Program, Scientific Results, Leg 120*. ODP, College Station, Texas, pp. 785–810.
- Lee, J.I., Park, B.-K., Jwa, Y.-J., Yoon, H.I., Yoo, K.C., Kim, Y., 2005. Geochemical characteristics and the provenance of sediments in the Bransfield Strait, West Antarctica. *Marine Geology* 219, 81–98.
- Lisiecki, L.E., Raymo, M.E., 2005. A Pliocene–Pleistocene stack of 57 globally distributed benthic  $\delta^{18}O$  records. *Paleoceanography* 20, PA1003.
- Machado, A., Chemale Jr., F., Conceição, R.V., Kawaskita, K., Morata, D., Oteiza, O., Van Schmus, W.R., 2005a. Modeling of subduction components in the Genesis of the Meso-Cenozoic igneous rocks from the South Shetland Arc, Antarctica. *Lithos* 82, 435–453.
- Machado, A., Lima, E.F., Chemale Jr., F., Morata, D., Oteiza, O., Almeida, D.P.M., Figueiredo, A.M.G., Alexandre, F.M., Urrutia, J.L., 2005b. Geochemistry constraints of Mesozoic–Cenozoic calc-alkaline magmatism in the South Shetland arc, Antarctica. *Journal of South American Earth Sciences* 18, 407–425.
- Martinson, D.G., Pisias, N.G., Hays, J.D., Imbrie, J., Moore Jr., T.C., Shackleton, N.J., 1987. Age dating and the orbital theory of the ice ages: development of a high-resolution 0 to 300,000-year chronostratigraphy. *Quaternary Research* 27, 1–29.
- Masson-Delmotte, V., Stenni, B., Pol, K., Braconnot, P., Cattani, O., Falourd, S., Kageyama, M., Jouzel, J., Landais, A., Minster, B., Barnola, J.M., Chappellaz, J., Krinner, G., Johnsen, S., Röthlisberger, R., Hansen, J., Mikolajewicz, U., Otto-Bliesner, B., 2010. EPICA Dome C record of glacial and interglacial intensities. *Quaternary Science Reviews* 29, 113–128.
- McIntyre, L., Kaczmarzka, I., 1996. Improved resolution of the Pleistocene extinction level of *Stylatractus universus* Hays (Radiolaria) in ODP Hole 745B, Kerguelen Plateau. *Micropaleontology* 42, 375–379.
- Nelson, B.K., DePaolo, D.J., 1988. Application of Sm–Nd and Rb–Sr isotopic systematic to studies of provenance and basin analysis. *Journal of Sedimentary Petrology* 58, 348–357.
- Nereson, N.A., Waddington, E.D., Raymond, C.F., Jacobson, H.P., 1996. Predicted age-depth scales for Siple Dome and Inland WAIS Ice Cores in west Antarctica. *Geophysical Research Letters* 23, 3163–3166.
- Nowlin Jr., W.D., Zenk, W., 1988. Westward currents along the margin of the South Shetland Island Arc. *Deep Sea Research* 35, 269–301.
- Orsi, A.H., Whitworth III, T., Nowlin Jr., W.D., 1995. On the meridional extent and fronts of the Antarctic Circumpolar Current. *Deep Sea Research I: Oceanographic Research Papers* 42, 641–673.
- Pearce, J.A., 1983. Role of the sub-continental lithosphere in magma genesis at active continental margins. In: Hawkesworth, C.J., Norry, M.J. (Eds.), *Continental basalts and mantle xenoliths*. Shiva, Nantwich, pp. 230–249.
- Pudsey, C.J., 1992. Late Quaternary changes in Antarctic Bottom Water velocity inferred from sediment grain size in the northern Weddell Sea. *Marine Geology* 107, 9–33.
- Reimer, P.J., Baillie, M.G.L., Bard, E., Bayliss, A., Beck, J.W., Blackwell, P.G., Bronk Ramsey, C., Buck, C.E., Burr, G.S., Edwards, R.L., Friedrich, M., Grootes, P.M., Guilderson, T.P., Hajdas, I., Heaton, T.J., Hogg, A.G., Hughen, K.A., Kaiser, K.F., Kromer, B., McCormac, F.G., Manning, S.W., Reimer, R.W., Richards, D.A., Southon, J.R., Talamo, S., Turney, C.S.M., van der Plicht, J., Weyhenmeyer, C.E., 2009. IntCal09 and Marine09 radiocarbon age calibration curves, 0–50,000 years cal BP. *Radiocarbon* 51, 1111–1150.
- Roy, M., van de Flierdt, T., Hemming, S.R., Goldstein, S.L., 2007.  $^{40}Ar/^{39}Ar$  ages of hornblende grains and bulk Sm/Nd isotopes of circum-Antarctic glacio-marine sediments: implications for sediment provenance in the southern ocean. *Chemical Geology* 244, 507–519.
- Saunders, A.D., Tarney, J., Weaver, S.D., 1980. Transverse geochemical variations across the Antarctic Peninsula: implications for the genesis of calc-alkaline magmas. *Earth and Planetary Science Letters* 46, 344–360.
- Savidge, D., Amft, J.A., 2009. Circulation on the West Antarctic Peninsula derived from 6 years of shipboard ADCP transects. *Deep Sea Research I: Oceanographic Research Papers* 56, 1633–1655.
- Tarney, J., Weaver, S.D., Saunders, A.D., Pankhurst, R.J., Barker, P.F., 1982. Volcanic eruption of the northern Antarctic Peninsula and the Scotia Arc. In: Thorpe, R.S. (Ed.), *Andesites*. John Wiley, Chichester, pp. 328–333.
- Taylor, S.R., McLennan, S.M., 1985. *The continental Crust: its Composition and Evolution*. Blackwell Science, Oxford, 312 pp.
- Thomson, M.R.A., Pankhurst, R.J., 1983. Age of post-Gondwanan calc-alkaline volcanism in the Antarctic Peninsula region. In: Oliver, R.L., James, P.R., Jago, J.B. (Eds.), *Antarctic Earth Science*. Australian Academy of Science, Canberra, pp. 328–333.
- Tucholke, B.E., 1977. Sedimentation processes and acoustic stratigraphy in the Bellingshausen Basin. *Marine Geology* 25, 209–230.
- van de Flierdt, T., Goldstein, S.L., Hemming, S.R., Roy, M., Frank, M., Halliday, A.N., 2007. Global neodymium-hafnium isotope systematics-revisited. *Earth and Planetary Science Letters* 259, 432–441.
- Walter, H.J., Hegner, E., Diekmann, B., Kuhn, G., Rutgers van der loeff, M.M., 2000. Provenance and transport of terrigenous sediment in the South Atlantic Ocean and their relations to glacial and interglacial cycles: Nd and Sr isotopic evidence. *Geochimica et Cosmochimica Acta* 64, 3813–3827.
- Wasserburg, G.J., Jacobson, S.B., Depaolo, D.J., McCulloch, M.T., Wen, T., 1981. Precise determination of Sm/Nd ratios, Sm and Nd isotopic abundances in standard solutions. *Geochimica et Cosmochimica Acta* 45, 2311–2323.
- Whitworth III, T., Nowlin Jr., W.D., Worley, S.J., 1982. The net transport of the Antarctic Circumpolar Current through Drake Passage. *Journal of Physical Oceanography* 12, 960–971.
- Williams, T., van de Flierdt, T., Hemming, S., Chung, E., Roy, M., Goldstein, S.L., 2010. Evidence for iceberg armadas from East Antarctica in the Southern Ocean during the late Miocene and early Pliocene. *Earth and Planetary Science Letters* 290, 351–361.
- Yoon, H.I., Yoo, K.-C., Bak, Y.-S., Lee, Y.I., Lee, J.I., 2009. Core-based reconstruction of paleoenvironmental conditions in the southern Drake Passage (West Antarctica) over the last 150 ka. *Geo-Marine Letters* 29, 309–320.